System Strength Sensitivity to Power Flow Perturbations in AC Power Systems with Inverter-based Resources

Trager Joswig-Jones[*†], Baosen Zhang[†], Shuan Dong[*], Jin Tan[*],
[*]Power Systems Engineering Center, National Renewable Energy Laboratory (NREL), Golden, CO, USA
[†]Department of Electrical and Computer Engineering, University of Washington, Seattle, WA, USA
Emails: {joswitra, zhangbao}@uw.edu, {shuan.dong, jin.tan}@nrel.gov

***Abstract*—As inverter-based resources (IBRs) contribute larger shares of generation in electrical power grids, their impact on the stability of these systems grows. Quantifying the strength of the system is important for identifying potential stability issues related to IBRs. Recently, new admittance model based system strength metrics have been proposed to identify stability issues and control interactions in systems with high levels of IBRs; however, these methods depend on the linearization of nonlinear devices in power systems and must be evaluated at many operating points to understand how the state of the system impacts system strength. In this paper, we propose new system strength metrics based on the sensitivity of the small-signal stability of the system to changes in the operating point due to perturbations in power injections. We validate our approach on a 14-bus test system to show how the metrics can be used to find remedial actions for small-signal stability issues.**

***Index Terms*—Grid strength, inverter-based resource, power flow, power system stability, system strength**

I. Introduction

As electrical power systems are becoming more reliant on inverter-based resources (IBRs), grid operators are faced with a range of new challenges when ensuring power systems can maintain stable voltage and frequency. The integration of conventional grid-following (GFL) IBRs into power systems can make the system more prone to small-signal instability such as subsynchronous oscillations [1], [2], which have been observed in power systems repeatedly over the past decade. The ability of power systems to maintain a stable voltage and frequency under disturbances can broadly be referred to as system strength [3], and many metrics have been developed that quantify this system strength to screen the grid for weak areas and identify potential modes of instability.

Traditionally used grid strength metrics, such as short-circuit ratio (SCR), cannot accurately quantify system strength for systems with high IBR penetration and can fail to identify areas with low system strength [3]. In addition to this shortfall, SCR and other methods that rely on steady-state or short-circuit analysis cannot consider instability caused by control interactions between IBR devices [4]. Consequently, new metrics have been proposed, including admittance-based methods that directly consider small-signal stability [5]–[7]. While approaches that estimate small-signal stability regions [8], [9] or trace eigenvalue paths [10] may not be practical for screening large systems with IBRs, metrics based on the frequency response or sensitivity of modes can inform operators on how to control the system to prevent small-signal instability.

Previous studies have investigated methods for calculating the sensitivity of system eigenvalues to changes in device parameters [11], [12]. However, few consider the interactions between power flow parameters to allow for calculating sensitivities with respect to power injections or bus voltages. [13] considers how to calculate eigenvalue sensitivities with respect to perturbations in power flow parameters, but this method relies on white-box analytical device models and cannot be directly applied to systems containing proprietary, black-boxed IBRs. More recently, [14] employed grey-box modeling techniques to compute the sensitivity of eigenvalues to changes in parameters, but does not consider sensitivities to power flow parameters.

In this paper, we define new system strength metrics that extend the work in [7], [14] to consider the sensitivity of the system eigenvalues to changes in the system power flow due to perturbations in bus power injections. We demonstrate with a 14-bus test system, how such an approach can provide system operators with information to practically identify and mitigate small-signal stability challenges in real-time by redispatching generators in the system.

The remainder of this paper is organized as follows. Section II introduces the system model. Section III-A discusses how to find the sensitivity of the power flow to perturbations in power flow parameters and Section III-B discusses how to use these sensitivities to calculate the sensitivities of the system's eigenvalues. Section III-C defines system strength metrics based on these power injection sensitivities and Section III-D discusses their scalability. Section IV demonstrates the capabilities of these metrics with a 14-bus test system and Section V concludes the paper.

This work was authored in part by NREL for the U.S. Department of Energy (DOE) under Contract No. DE-AC36-08GO28308. Funding for the NREL authors provided by U.S. Department of Energy Office of Energy Efficiency and Renewable Energy Solar Energy Technologies Office. The views expressed in the article do not necessarily represent the views of the DOE or the U.S. Government.

979-8-3315-8138-1

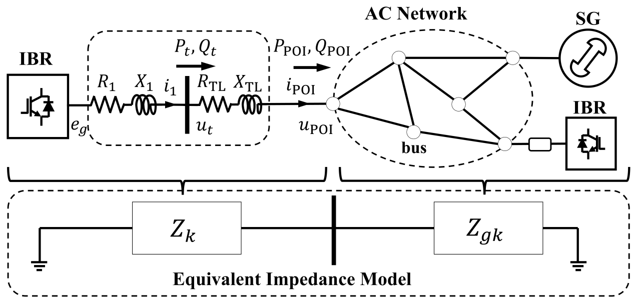

Fig. 1: Illustration of a power system with its equivalent impedance model.

II. System Model

We consider a system of devices connected in an AC network. A representation of such a network can be seen in Fig. 1. The network is defined with a set of N buses $\mathcal{N}$ and lines $\mathcal{E}$, where $Y_{ik} = G_{ik} + jB_{ik}$ denotes the admittance between buses i and k. Bus $i \in \mathcal{N}$ is characterized by power injections $S_i = P_i + jQ_i$ and voltage $V_i\angle\theta_i$; these are collected into vectors $\mathbf{V}, \mathbf{\Theta}, \mathbf{P}, \mathbf{Q}$. A slack bus maintains system power balance by varying its power injections.

A. Power Flow

In steady-state, the power flow through the network satisfies the AC power flow equations

$$P_i = V_i \sum_{i \sim k} V_k (G_{ik} \cos\theta_{ik} + B_{ik} \sin\theta_{ik}), \tag{1a}$$

$$Q_i = V_i \sum_{i \sim k} V_k (G_{ik} \sin\theta_{ik} - B_{ik} \cos\theta_{ik}), \tag{1b}$$

for each bus $i \in \mathcal{N}$. The first-order Taylor series expansion of (1) gives

$$\begin{bmatrix} \Delta\mathbf{P} \\ \Delta\mathbf{Q} \end{bmatrix} = J(\mathcal{M}) \begin{bmatrix} \Delta\mathbf{V} \\ \Delta\mathbf{\Theta} \end{bmatrix}, \quad J(\mathcal{M}) = \begin{bmatrix} \frac{\partial\mathbf{P}}{\partial\mathbf{V}} & \frac{\partial\mathbf{P}}{\partial\mathbf{\Theta}} \\ \frac{\partial\mathbf{Q}}{\partial\mathbf{V}} & \frac{\partial\mathbf{Q}}{\partial\mathbf{\Theta}} \end{bmatrix}, \tag{2}$$

where J is the Jacobian typically used to solve the power flow problem. Here we denote the power flow parameters at all buses in the system as $\mathcal{M}$, where $\mathcal{M}_i = [P_i, Q_i, V_i, \Theta_i]$ are the power flow parameters at bus i.

To solve power flow models, buses are specified as having two of their four power flow parameters being fixed. Typically, bus types are *PQ*, *PV*, and *V*Θ (the slack bus) where the bus type indicates the parameters that are fixed at that bus. We let $\overline{\mathcal{V}}$, $\overline{\Theta}$, $\overline{\mathcal{P}}$, and $\overline{\mathcal{Q}}$ denote the set of buses where the respective parameter is fixed at that bus and we let $\widetilde{\mathcal{V}}$, $\widetilde{\Theta}$, $\widetilde{\mathcal{P}}$, and $\widetilde{\mathcal{Q}}$ denote the set of buses where the respective parameter value is variable at that bus and depends on the fixed values and (1).

B. Dynamics and Small-Signal Stability

The dynamics of the devices and lines in the system are represented using nonlinear models in dq reference frames. Linearizing these models around an operating point satisfying the power flow equations yields equivalent admittance/impedance models, which are transfer functions relating voltage $\mathbf{V}_{i,\mathrm{dq}}$ and current $\mathbf{I}_{i,\mathrm{dq}}$ at the point of interconnection (POI). Aligning these models to a global dq frame, they can be combined to form a whole-system admittance model, a frequency-domain transfer function matrix that characterizes the small-signal dynamic characteristics of the entire system [15].

The whole-system admittance matrix is defined as

$$\hat{\mathbf{Y}}(s) = (I + \mathbf{Y}_{\mathrm{net}}(s)\mathbf{Z}(s))^{-1}\mathbf{Y}_{\mathrm{net}}, \tag{3}$$

where $\mathbf{Y}_{\mathrm{net}}(s)$ is the nodal admittance matrix of the network and $\mathbf{Z}(s) = diag(Z_1(s), Z_2(s), \ldots, Z_K(s))$ is the block diagonal matrix containing the device impedances. The poles of each element of $\hat{\mathbf{Y}}(s)$ are equivalent to the eigenvalues of the system [15]. If all of the eigenvalues lie in the left hand plane, then the system is small-signal stable. Further, as discussed in [14], the sensitivity of these eigenvalues is related to $\hat{\mathbf{Y}}(s)$ as $\frac{\partial\lambda}{\partial\hat{\mathbf{Y}}^{-1}(\lambda)} = -\mathrm{Res}_\lambda\hat{\mathbf{Y}}$ and the perturbation of these eigenvalues with respect to sufficiently small perturbations in $\hat{\mathbf{Y}}(s)$ is

$$\Delta\lambda = \langle -\mathrm{Res}^*_\lambda\hat{\mathbf{Y}}, \Delta\hat{\mathbf{Y}}^{-1} \rangle, \tag{4}$$

where $\langle\cdot,\cdot\rangle$ is the Frobenius inner product of two matrices, $\mathrm{Res}_\lambda\hat{\mathbf{Y}}$ is the residue of the whole-system admittance matrix evaluated at λ, and $*$ denotes the conjugate transpose [16].

Admittance models vary with the system operating point due to the linearization of nonlinear devices. Consequently, changes in a device's power injection or POI voltage shift the linearization point and the resulting equivalent impedance, ultimately altering system eigenvalues.

III. Method

A. Power Flow Sensitivity

When the power injection at a bus changes, the system adjusts to a new power flow solution satisfying (1). Accurately assessing the impact of such a perturbation on small-signal stability requires accounting for its effect on the overall power flow [13]. Although this nonlinear problem is generally challenging, for sufficiently small perturbations it can be approximated using a first-order expansion. In this section we discuss how to calculate the power flow perturbation $\Delta\mathcal{M}$ for a perturbation to a chosen fixed power flow parameter Δx (e.g. for a perturbation in the active power at bus 2 set $x = P_2$).

First, we partition the Jacobian relating to whether or not a power flow parameter is fixed or variable and define submatrices as shown in (5).

$$J = \left[\begin{array}{cc|cc} \frac{\partial\overline{\mathbf{P}}}{\partial\overline{\mathbf{V}}} & \frac{\partial\overline{\mathbf{P}}}{\partial\overline{\mathbf{\Theta}}} & \frac{\partial\overline{\mathbf{P}}}{\partial\widetilde{\mathbf{V}}} & \frac{\partial\overline{\mathbf{P}}}{\partial\widetilde{\mathbf{\Theta}}} \\ \frac{\partial\overline{\mathbf{Q}}}{\partial\overline{\mathbf{V}}} & \frac{\partial\overline{\mathbf{Q}}}{\partial\overline{\mathbf{\Theta}}} & \frac{\partial\overline{\mathbf{Q}}}{\partial\widetilde{\mathbf{V}}} & \frac{\partial\overline{\mathbf{Q}}}{\partial\widetilde{\mathbf{\Theta}}} \\ \hline \frac{\partial\widetilde{\mathbf{P}}}{\partial\overline{\mathbf{V}}} & \frac{\partial\widetilde{\mathbf{P}}}{\partial\overline{\mathbf{\Theta}}} & \frac{\partial\widetilde{\mathbf{P}}}{\partial\widetilde{\mathbf{V}}} & \frac{\partial\widetilde{\mathbf{P}}}{\partial\widetilde{\mathbf{\Theta}}} \\ \frac{\partial\widetilde{\mathbf{Q}}}{\partial\overline{\mathbf{V}}} & \frac{\partial\widetilde{\mathbf{Q}}}{\partial\overline{\mathbf{\Theta}}} & \frac{\partial\widetilde{\mathbf{Q}}}{\partial\widetilde{\mathbf{V}}} & \frac{\partial\widetilde{\mathbf{Q}}}{\partial\widetilde{\mathbf{\Theta}}} \end{array}\right] = \left[\begin{array}{c|c} J_{-,-} & J_{-,\sim} \\ \hline J_{\sim,-} & J_{\sim,\sim} \end{array}\right] \tag{5}$$

Here $J_{-,\sim}$ represents the mapping of variable voltage parameters, $(\widetilde{\mathcal{V}}, \widetilde{\Theta})$, to fixed power parameters, $(\overline{\mathcal{P}}, \overline{\mathcal{Q}})$. We further define $J_{-,\bullet} = [J_{-,-}, J_{-,\sim}]$, which selects the rows of J corresponding to fixed power injections and the columns corresponding to all voltage values.

979-8-3315-8138-1

For a perturbation in the active power at buses in $\overline{\mathcal{P}}$ or reactive power at buses in $\overline{\mathcal{Q}}$ ($x = P_i, i \in \overline{\mathcal{P}}$ or $x = Q_i, i \in \overline{\mathcal{Q}}$) we can calculate the voltage magnitude and angle sensitivities at buses in $\widetilde{\mathcal{V}}$ and $\widetilde{\Theta}$, respectively, from $(\frac{\partial \mathbf{P}}{\partial x}, \frac{\partial \mathbf{Q}}{\partial x}) = J(\frac{\partial \mathbf{V}}{\partial x}$ $\frac{\partial \boldsymbol{\Theta}}{\partial x})$ by taking $\frac{\partial \overline{\mathbf{V}}}{\partial x}, \frac{\partial \overline{\boldsymbol{\Theta}}}{\partial x} = \mathbf{0}$ to get

$$\begin{bmatrix} \frac{\partial \widetilde{\mathbf{V}}}{\partial x} \\ \frac{\partial \widetilde{\boldsymbol{\Theta}}}{\partial x} \end{bmatrix} = J^{-1}_{-,\sim} \begin{bmatrix} \frac{\partial \overline{\mathbf{P}}}{\partial x} \\ \frac{\partial \overline{\mathbf{Q}}}{\partial x} \end{bmatrix}. \tag{6}$$

We can then calculate the sensitivities of $\widetilde{\mathbf{P}}, \widetilde{\mathbf{Q}}$ as

$$\begin{bmatrix} \frac{\partial \widetilde{\mathbf{P}}}{\partial x} \\ \frac{\partial \widetilde{\mathbf{Q}}}{\partial x} \end{bmatrix} = J_{\sim,\bullet} \begin{bmatrix} \frac{\partial \mathbf{V}}{\partial x} \\ \frac{\partial \boldsymbol{\Theta}}{\partial x} \end{bmatrix}. \tag{7}$$

We then combine these sensitivities to get $\frac{\partial \mathcal{M}_i}{\partial x} = [\frac{\partial P_i}{\partial x}, \frac{\partial Q_i}{\partial x}, \frac{\partial V_i}{\partial x}, \frac{\partial \Theta_i}{\partial x}]$ for each bus in the system.

B. Eigenvalue Perturbations

We now use the power flow perturbations to compute changes in the system eigenvalues. This requires the sensitivities $\frac{\partial Z_k}{\partial \mu}$ of the device impedances with respect to local power flow parameters. Equivalent device impedances and these sensitivities can be obtained from analytical models or from frequency-scanning measurements, as described in [14]. Because most black-box inverter models allow specification of power references, this approach is also compatible with black-box modeling when using frequency scanning to obtain device admittance models.

Using the power flow sensitivities we can determine the perturbation to a device's equivalent impedance for a perturbation in a power flow parameter x as

$$\Delta_x Z_k = \sum_{\mu \in \mathcal{M}_k} \frac{\partial Z_k}{\partial \mu} \frac{\partial \mu}{\partial x} \cdot \Delta x. \tag{8}$$

Then using (3) and (4), noting that $\Delta \hat{\mathbf{Y}}^{-1} = \Delta \mathbf{Z}$ (See Appendix A for proof) we can calculate the perturbation to the system eigenvalue λ as

$$\Delta_x \lambda = \langle -\mathrm{Res}^*_\lambda \hat{\mathbf{Y}}, \Delta_x \mathbf{Z} \rangle. \tag{9}$$

This is equivalent to $\Delta_x \lambda = \sum_{k \in \mathcal{N}} \langle -\mathrm{Res}^*_\lambda \hat{\mathbf{Y}}_{kk}, \Delta_x Z_k \rangle$, where $\hat{\mathbf{Y}}_{kk}$ are diagonal blocks of $\hat{\mathbf{Y}}$, which can be calculated from the local device impedance and the grid impedance seen from that device's POI [14].

C. Small-Signal Stability Metrics

In this section we define system strength metrics based on the eigenvalue sensitivity with respect to perturbations in power injections. We define the power flow sensitivity index for an eigenvalue λ and parameter μ at bus i as

$$\mu \mathrm{SI}_{i,\lambda} = \frac{\mathrm{re}(\Delta_\mu \lambda)}{|\mathrm{re}(\lambda)|}. \tag{10}$$

This normalizes the sensitivity of the real part of an eigenvalue by the magnitude of the real part of that eigenvalue. The smaller the real part of an eigenvalue and the higher its sensitivity, the larger the sensitivity index will be. From this we can consider the maximum normalized eigenvalue shift towards the right hand plane for an increase (to) or decrease (from) in the power value and define the to sensitivity index (μTSI) and from sensitivity index (μFSI) as

$$\mu \mathrm{TSI}_i = \max_\lambda (\mu \mathrm{SI}_{i,\lambda}), \quad \mu \mathrm{FSI}_i = \max_\lambda (-\mu \mathrm{SI}_{i,\lambda}). \tag{11}$$

The inverse of the μTSI and μFSI sensitivity indices give a first-order approximate of how large a perturbation to the parameter can be before the eigenvalue will cross into the RHP and the system will become unstable. With this intuition, it is clear that a larger sensitivity indicates a weaker system which we show in the simulation results in the following section.

D. Scalability

This sensitivity-based approach is significantly faster than recalculating the full system eigenvalues at a perturbed operating point, as it leverages system residues to compute sensitivities through simple linear algebraic operations. Utilizing selective eigenvalue algorithms [17] to acquire the base eigenvalues and sparse state-space representations to avoid the numerical precision challenges of high-order transfer function matrices allows the method to be applied to large-scale systems. Acquiring equivalent admittance models and their sensitivities from black-box models through vector fitting [18] is the most intensive step; however, these device-level admittances are independent and can be calculated in parallel or pre-calculated offline for a range of operating points.

IV. Case Study

We perform a case study to validate the eigenvalue sensitivity calculations and test the performance of our proposed metrics in identifying weak buses and informing remedial actions. We choose to focus on perturbations to fixed active and reactive power injections and model all buses other than the slack bus as *PQ* buses. We use a modified IEEE 14-bus system where the synchronous condensers are replaced by identical GFL IBRs, with one additional IBR at bus 10, as shown in Fig. 2. The inverters are all selected to have identical GFL control schemes and vary their current injections to align with active and reactive power set points. Next, we compare different generation cases detailed in Table I.
This case study uses a modified version of the Simplus Grid

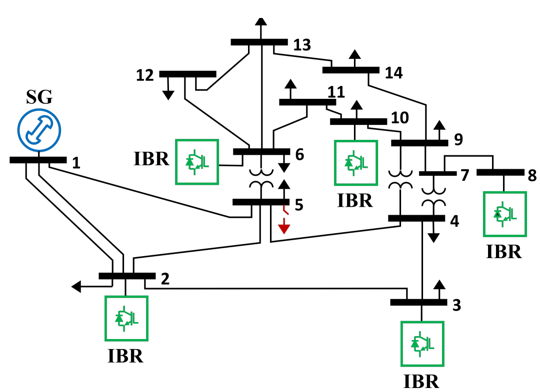

Fig. 2: Diagram of the modified IEEE 14-bus test system.

979-8-3315-8138-1

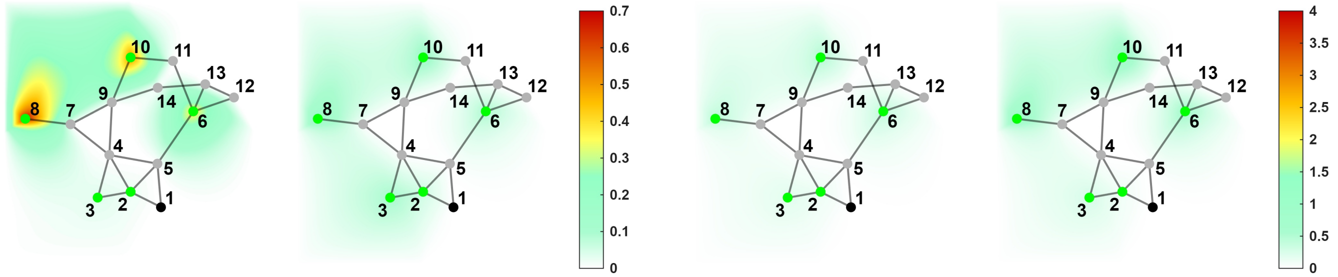

(a) PTSI (b) PFSI (c) QTSI (d) QFSI

Fig. 3: 14-bus system base case generator active and reactive power injection sensitivities.

TABLE I
IEEE 14-BUS CASE STUDY CASE DESCRIPTIONS

Case	Changes from Base Case
Case A	$P_G : 0.5 \rightarrow 1.2$ pu at bus **8** and bus **10**
Case B	$P_G : 0.5 \rightarrow 1.2$ pu at bus **6** and bus **10**
Case A-2	$P_G : 0.5 \rightarrow 1.2$ pu at bus **8** and bus **10**, $Q_G : 0.05 \rightarrow 0.5$ pu at bus **8**.
Case A-3	$P_G : 0.5 \rightarrow 1.2$ pu at bus **8** and bus **10**, Bus **8** GFL to GFM control.

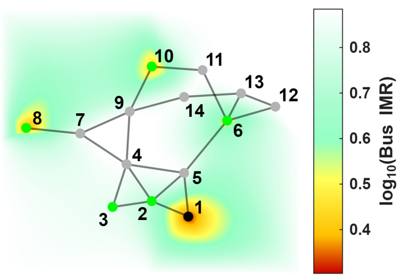

Fig. 4: 14-bus system base case IMR values.

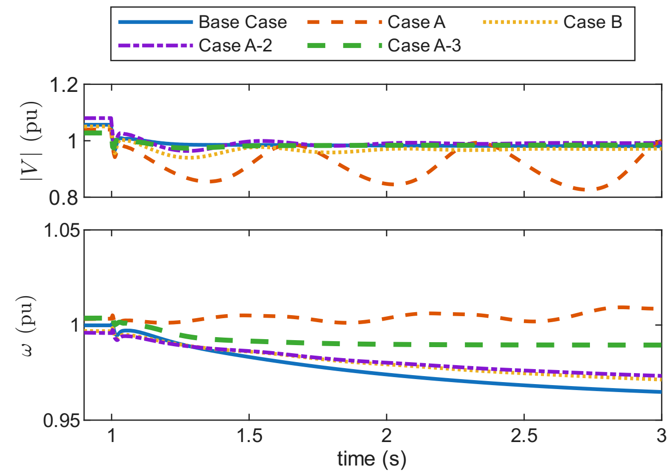

Fig. 5: Time-domain response of bus 10 voltage magnitude and frequency for the cases in Table I. A 0.67 pu load step at bus 5 occurs at $t = 1$ s. Case A exhibits an undamped 1.4 Hz oscillation, which is not prevalent in Case B. Increasing reactive power injected at bus 8 (Case A-2) or changing its control from GFL to GFM (Case A-3) mitigate the oscillation introduced in Case A.

Tool [19], and the code used to produce these results will be made available at https://github.com/TragerJoswig-Jones/Simplus-Grid-Tool-Power-Flow-Sensitivity.

A. 14-Bus Test System Results

First, we validate that the proposed methodology for calculating eigenvalue perturbations produces accurate results. We calculate the actual eigenvalue perturbations by perturbing the power injection at a bus, calculating the new steady-state power flow for the system, and then computing the resulting eigenvalue perturbation. As shown in Table II, the actual and predicted eigenvalue perturbations align closely.

Next, we calculate the proposed power flow sensitivity metrics proposed in Section III-C with a selection of eigenvalues for the Base Case scenario. We also plot the system's Impedance Margin Ratio (IMR) values in Fig. 4, and compare this to our metrics shown in Fig. 3. We see that IBR buses identified as weak by IMR are also identified as being weak by the PTSI and QFSI metrics; however, these metrics link this weakness to shifts in power injections at these buses. Although similar to IMR in their use of admittance residues, the proposed metrics distinguish themselves by linking eigenvalue sensitivities directly to power flow perturbations rather than relying on conservative, worst-case impedance margins.

Next, we apply increases in active power injection at buses with differing PTSI values and simulate the nonlinear time-domain system to see how this impacts its response to a step in the active power load at bus 5. Both cases increase the power injection at bus 10, but Case A increases generation at the more sensitive bus 8 IBR and Case B selects the less sensitive IBR at bus 6. Fig. 5 shows that the increase in power injected at bus 8 with the higher PTSI value results in a maintained oscillation post-disturbance, while the same increase in power injected at the less sensitive bus 6 results in the system maintaining adequate damping of this mode.

TABLE II
COMPARISON OF PREDICTED AND ACTUAL EIGENVALUE PERTURBATIONS FOR THREE MODES OF THE BASE CASE 14-BUS TEST SYSTEM.

Perturbation		λ = -1.011 + 0.000j	λ = -10.791 + 3.382j	λ = -6.969 + 377.858j
$\Delta\mu \times 10^5$		$\Delta\lambda \times 10^5$	$\Delta\lambda \times 10^5$	$\Delta\lambda \times 10^5$
$\Delta P_2 = 1$ pu	Actual	4.905 + 0.000j	-0.582 - 0.699j	0.000 + 0.002j
	Pred.	4.911 + 0.000j	-0.583 - 0.700j	0.000 + 0.001j
$\Delta Q_2 = 1$ pu	Actual	11.844 + 0.000j	1.312 + 0.847j	-0.007 + 0.005j
	Pred.	11.838 + 0.000j	1.312 + 0.847j	-0.008 + 0.005j
$\Delta P_8 = 1$ pu	Actual	1.362 + 0.000j	0.901 - 1.013j	0.003 + 0.000j
	Pred.	1.359 + 0.000j	0.900 - 1.013j	0.003 - 0.001j
$\Delta Q_8 = 1$ pu	Actual	24.841 + 0.000j	-1.344 + 0.215j	-0.022 + 0.010j
	Pred.	24.830 + 0.000j	-1.344 + 0.215j	-0.022 + 0.012j

979-8-3315-8138-1

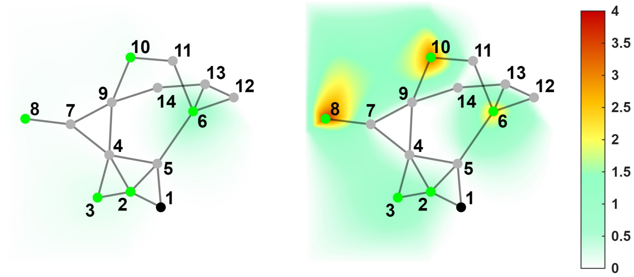

(a) QTSI (b) QFSI

Fig. 6: 14-bus generator reactive power injection sensitivities for case A.

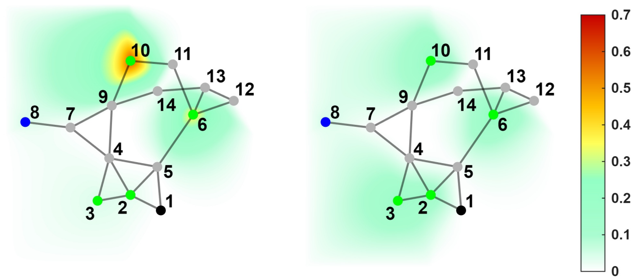

(a) PTSI (b) PFSI

Fig. 7: 14-bus generator active power injection sensitivities for base case with GFM IBR control at bus 8.

Lastly, we explore two remedial actions to mitigate the subsynchronous oscillation introduced in Case A. Our first action is informed by looking at the reactive power sensitivities for Case A in Fig. 6. According to the QFSI values, an increase in the reactive power injection at bus 8 will result in some eigenvalue shifting to the left and increase the damping of its associated mode. The QTSI value at bus 8 being low indicates that this increase will not significantly shift any eigenvalues towards the right. Following this, in Case A-2 we increase the reactive power injection of the IBR at bus 8 and observe a significant increase in the damping of the oscillatory mode in Fig. 5. Next in Case A-3, we change the control mode of the IBR at bus 8 from GFL to a grid-forming (GFM) droop controller and plot the active power sensitivity injections for the Base Case in Fig. 7. Fig. 7a shows that the system is no longer sensitive to increases in active power injection at bus 8, which we validate by simulating Case A with GFM control at bus 8 and seeing an improved response in Fig. 5.

V. Conclusion

This paper presents a method to compute power flow sensitivities from perturbations in power injections and use these sensitivities to determine the sensitivities of an AC power system's eigenvalues. We define grid strength metrics based on these eigenvalue sensitivities to bus power injections, and demonstrate the capabilities of these metrics with a 14-bus test system. These metrics can be used to screen dispatches and identify remedial actions for small-signal stability issues. Future work includes investigating voltage magnitude sensitivities, applying this approach to look at the sensitivities of the system to changes in power electronic loads, and considering how frequency and voltage droop parameters impact resulting power flow perturbations.

Appendix

A. Device Impedance Perturbation Proof

For a small change $\Delta\mathbf{Z}(s)$ in $\mathbf{Z}(s)$ we have

$$\begin{aligned}&\hat{\mathbf{Y}}(s)^{-1} + \Delta\hat{\mathbf{Y}}(s)^{-1} \\ &= ((I + \mathbf{Y}_{\text{net}}(s)(\mathbf{Z}(s) + \Delta\mathbf{Z}(s)))^{-1}\mathbf{Y}_{\text{net}})^{-1} \\ &= \mathbf{Y}_{\text{net}}^{-1} + \mathbf{Z}(s) + \Delta\mathbf{Z}(s).\end{aligned} \tag{12}$$

Using the inverse of (3) we can substitute in $\hat{\mathbf{Y}}(s)^{-1}$ to find $\Delta\hat{\mathbf{Y}}(s)^{-1} = \Delta\mathbf{Z}(s)$.

References

[1] S.-H. Huang, J. Schmall, J. Conto, J. Adams, Y. Zhang, and C. Carter, "Voltage control challenges on weak grids with high penetration of wind generation: Ercot experience," in *2012 IEEE Power and Energy Society General Meeting*, 2012, pp. 1–7.

[2] Y. Cheng *et al.*, "Real-world subsynchronous oscillation events in power grids with high penetrations of inverter-based resources," *IEEE Trans. Power Syst.*, vol. 38, no. 1, pp. 316–330, 2023.

[3] CIGRE Working Group B4.62, "Connection of wind farms to weak ac networks," *Technical Brochure 671*, 2016.

[4] C. Henderson, A. Egea-Alvarez, T. Kneuppel, G. Yang, and L. Xu, "Grid strength impedance metric: An alternative to SCR for evaluating system strength in converter dominated systems," *IEEE Trans. Power Del.*, vol. 39, no. 1, p. 386–396, Feb. 2024.

[5] T. Joswig-Jones, S. Dong, D. Wu, and J. Tan, "A review of system strength metrics for inverter-based power systems," 2026, in review - submitted to PES-GM 2026.

[6] F. Ma, H. Xin, D. Wu, Y. Liu, and X. Chen, "Assessing small-signal grid strength of 100% inverter-based power systems," *IEEE Trans. Power Del.*, vol. 39, no. 5, p. 2784–2796, Oct. 2024.

[7] Y. Zhu, T. C. Green, X. Zhou, Y. Li, D. Kong, and Y. Gu, "Impedance margin ratio: A new metric for small-signal system strength," *IEEE Trans. Power Syst.*, vol. 39, no. 6, p. 7291–7303, Nov. 2024.

[8] C. Qin and Y. Yu, "Small signal stability region of power systems with dfig in injection space," *Journal of Modern Power Systems and Clean Energy*, vol. 1, no. 2, pp. 127–133, 2013.

[9] L. Ding, Y. Men, Y. Du, X. Lu, B. Chen, J. Tan, and Y. Lin, "Region-based stability analysis of resilient distribution systems with hybrid grid-forming and grid-following inverters," in *2020 IEEE Energy Conversion Congress and Exposition (ECCE)*, 2020, pp. 3733–3740.

[10] A. Bouterakos, J. McKeon, and G. Tzounas, "On the eigenvalue tracking of large-scale systems," 2025. [Online]. Available: https://arxiv.org/abs/2504.17571

[11] H. Zein El-Din and R. Alden, "Second order eigenvalue sensitivities applied to power system dynamics," *IEEE Trans. Power App. Syst.*, vol. 96, no. 6, pp. 1928–1936, 1977.

[12] T. Smed, "Feasible eigenvalue sensitivity for large power systems," *IEEE Trans. Power Syst.*, vol. 8, no. 2, pp. 555–563, 1993.

[13] J. Ma, Z. Dong, and P. Zhang, "Eigenvalue sensitivity analysis for dynamic power system," in *2006 International Conference on Power System Technology*. Chongqing, China: IEEE, Oct. 2006, p. 1–7.

[14] Y. Zhu, Y. Gu, Y. Li, and T. C. Green, "Participation analysis in impedance models: The grey-box approach for power system stability," *IEEE Trans. Power Syst.*, vol. 37, no. 1, pp. 343–353, 2022.

[15] Y. Gu, Y. Li, Y. Zhu, and T. C. Green, "Impedance-based whole-system modeling for a composite grid via embedding of frame dynamics," *IEEE Trans. Power Syst.*, vol. 36, no. 1, p. 336–345, Jan. 2021.

[16] E. Stein and R. Shakarchi, *Complex Analysis*, ser. Princeton lectures in analysis. Princeton University Press, 2010.

[17] J. W. Demmel, *Applied Numerical Linear Algebra*. Philadelphia, PA: SIAM, 1997, ch. 7: Iterative Methods for Linear Systems, pp. 283–360.

[18] B. Gustavsen and A. Semlyen, "Rational approximation of frequency domain responses by vector fitting," *IEEE Trans. Power Del.*, vol. 14, no. 3, pp. 1052–1061, 1999.

[19] Y. Li, "Future-power-networks/simplus-grid-tool," 2021. [Online]. Available: https://github.com/Future-Power-Networks/Simplus-Grid-Tool

979-8-3315-8138-1